Preston, T. C., & Reid, J. P. (2015). Angular scattering of light by a homogeneous spherical particle in a zeroth-order Bessel beam and its relationship to plane wave scattering. *Journal of the Optical Society of America A*, *32*(6), 1053-1062. https://doi.org/10.1364/JOSAA.32.001053

Angular scattering of light by a homogeneous spherical particle in a zeroth-order Bessel beam and its relationship to plane wave scattering

April 11, 2015

Thomas C. Preston*[a] and Jonathan P. Reid[b]

[a]*Department of Atmospheric and Oceanic Sciences and Department of Chemistry, McGill University, 805 Sherbrooke Street West, Montreal, QC, Canada H3A 0B9*

[b]*School of Chemistry, University of Bristol, Cantock's Close, Bristol, UK, BS8 1TS*

submitted to the Journal of the Optical Society of America A

7 Figures, 1 Table and 18 manuscript pages

* Thomas C. Preston

e-mail: thomas.preston@mcgill.com

Abstract

The angular scattering of light from a homogeneous spherical particle in a zeroth-order Bessel beam is calculated using generalized Lorenz-Mie theory. We investigate the dependence of the angular scattering on the semi-apex angle of the Bessel beam and discuss the major features of the resulting scattering plots. We also compare Bessel beam scattering to plane wave scattering and provide criterion for when the difference between the two cases can be considered negligible. Finally, we discuss a method for characterizing spherical particles using angular light scattering. This work is useful to researchers who are interested in characterizing particles trapped in optical beams using angular dependent light scattering measurements.

OCIS Codes: (010.1110) Aerosols; (290.3030) Index measurements; (290.4020) Mie theory

1 Introduction

An accurate understanding of elastic light scattering by particles is important in many scientific fields. For over a hundred years, Lorenz-Mie theory (LMT)[1,2] has provided the foundation for qualitative and quantitative insight into a wide range of optical phenomena involving spherical particles,[3–7] among which the angular scattering of light has been one of the most important.[8,9] Computer code implementing LMT has been around for many decades (e.g. see Ref. 9, p. 477) and researchers can now calculate Mie coefficients in a computationally efficient manner.

However, even when restricted to the scattering of light by a spherical particle, calculations performed using the classical LMT may not accurately model experimental measurements. One of the most the common deficiencies of LMT is that the plane wave used in its formulation may not be suitable in describing the incident beam for the system of interest. This problem has been studied extensively, in particular for light scattering involving spherical particles in a Gaussian beam, and has led to the development of two popular theories which extend LMT to the case of an arbitrarily shaped beam.[10–17] These theories are mathematically equivalent and in both cases beam-shape coefficients are used to decompose the incident beam into partial waves.[14] Generalized Lorenz-Mie theory (GLMT)[11,14–17] will be used throughout this work, although many of the calculations were also verified using the theory of Barton *et al.*[10,12,13] (as expected, results from both theories were identical).

Optical Bessel beams have several properties that make their use in the manipulation and control of micron and sub-micron particles attractive: pseudo-nondiffracting, strong confinement forces in the transverse plane, and self-reconstruction.[18–22] In the field of aerosol science, Bessel beams are very appealing for the study of single aerosol particles and instrumentation

incorporating such beams has been recently demonstrated.[23–29] However, there remains the need for an approach to accurately characterize a particle once it has been trapped in such a beam. For a homogeneous spherical particle the radius and refractive index must be accurately determined. Whispering gallery modes that appear in cavity enhanced spectra are well-suited for this task,[30,31] but for sub-micron particles the spacing of these modes is often so large that the number of observable modes may be insufficient to simultaneously fit the refractive index and radius. While cavity enhanced Raman scattering has the requirement that the Raman bands are spectrally broad enough to contain an adequate number of whispering gallery modes, cavity enhanced fluorescence also has the limitation that particles will typically need to be doped with a dye and are susceptible to photobleaching.

In contrast, angular dependent measurements of elastic light scattering are not restricted in the above ways and can readily be made to determine the size of a sub-micron particle in an optical Bessel trap.[23–29] Such scattering will depend not only on radius and refractive index but also, in general, on the shape of the Bessel beam. Therefore, using LMT to model the scattering may not satisfactorily reproduce experimental results. Several groups have provided expressions for the beam-shape coefficients for a Bessel beam[20,32–34] and, in particular, the work of Taylor and Love should be highlighted. These authors derived analytical expressions for the beam-shape coefficients that do not contain any integrals and are valid outside of the paraxial approximation.[32] However, actual scattering calculations for a homogeneous sphere in a Bessel beam have been limited. Mitri published reports on light scattering of both zeroth- and higher-order Bessel beams[35,36] and, more recently, Li *et al.* used a non-paraxial description of a zeroth-order Bessel beam to study light scattering by a homogeneous sphere.[34] None of this work, though, considered systems that are relevant to the aerosol optical trapping discussed

above. Beyond the work on homogeneous spheres, elastic scattering of a zeroth-order optical Bessel beam from particles with anisotropic optical properties[37] and particles with a core-shell structure[38] have also recently been investigated.

Here, we focus on the angular dependent scattering of light by a homogeneous sphere in an optical zeroth-order Bessel beam. First, we give an overview of the angular dependent scattering as a function of the semi-apex angle of the Bessel beam (Section 3.1). Following that, we discuss systems of experimental interest to aerosol science and how the angular dependent scattering of a Bessel beam compares to that of a plane wave (Section 3.2). Finally, the suitability of approximating Bessel beam scattering with plane wave scattering for the purpose of characterizing spherical particles is examined (Section 3.3) and a new method for fitting both the radius and refractive index of a spherical particle is presented (Section 3.4).

2 Theory

In the non-paraxial (vectorial) description of a zeroth-order Bessel beam, the electric and magnetic fields (**E** and **H**) of the incident beam can be written as[20–22,39]

$$\mathbf{E}(\mathbf{r}) = E_0 e^{-ik_z z} \left\{ \begin{array}{l} [J_0(k_\perp \rho) + \beta^2 J_2(k_\perp \rho)\cos 2\phi]\hat{\mathbf{x}} \\ \beta^2 J_2(k_\perp \rho)\sin 2\phi\, \hat{\mathbf{y}} \\ i2\beta J_1(k_\perp \rho)\cos\phi\, \hat{\mathbf{z}} \end{array} \right\}, \tag{1}$$

$$\mathbf{H}(\mathbf{r}) = H_0 e^{-ik_z z} \left\{ \begin{array}{l} \beta^2 J_2(k_\perp \rho)\sin 2\phi\, \hat{\mathbf{x}} \\ [J_0(k_\perp \rho) - \beta^2 J_2(k_\perp \rho)\cos 2\phi]\hat{\mathbf{y}} \\ i2\beta J_1(k_\perp \rho)\sin\phi\, \hat{\mathbf{z}} \end{array} \right\}. \tag{2}$$

For a Bessel beam of wavenumber k and semi-apex angle θ_0, the longitudinal and transverse wavenumbers are $k_z = k\cos\theta_0$ and $k_\perp = k\sin\theta_0$, respectively (Fig. 1). Additionally, $\beta = \sin\theta_0/(1+\cos\theta_0)$, $\rho = \sqrt{x^2+y^2}$, and $\phi = \arctan(y/x)$. The relationship between the field amplitudes E_0 and H_0 is $E_0/H_0 = \sqrt{\mu/\epsilon}$ where ϵ is the permittivity and μ is the permeability of the medium. The time dependent factor of $e^{i\omega t}$ associated with the fields is omitted in this work. Finally, $\hat{\mathbf{x}}$, $\hat{\mathbf{y}}$, and $\hat{\mathbf{z}}$ are unit vectors in the cartesian coordinate system.

Scattering calculations were performed using GLMT.[11,14–17] The transverse electric $(g_l^m)_{\mathrm{TE}}$ and transverse magnetic $(g_l^m)_{\mathrm{TM}}$ beam-shape coefficients can be defined as two-dimensional integrals:[14]

$$(g_l^m)_{\mathrm{TE}} = \frac{-1}{4\pi}(i^{l-1})\frac{kr}{j_l(kr)}\frac{(l-|m|)!}{(l+|m|)!}\int_0^{2\pi}\int_0^{\pi}(H_{rad}(r,\theta,\phi)/H_0)P_l^{|m|}(\cos\theta)e^{-im\phi}\sin\theta d\theta d\phi, \tag{3}$$

$$(g_l^m)_{\mathrm{TM}} = \frac{-1}{4\pi}(i^{l-1})\frac{kr}{j_l(kr)}\frac{(l-|m|)!}{(l+|m|)!}\int_0^{2\pi}\int_0^{\pi}(E_{rad}(r,\theta,\phi)/E_0)P_l^{|m|}(\cos\theta)e^{-im\phi}\sin\theta d\theta d\phi, \tag{4}$$

where E_{rad} and H_{rad} are the radial components of the incident fields, j_l are spherical Bessel functions, $P_l^{|m|}$ are associated Legendre polynomials, and r is the radius at which integrals are evaluated. Eqs. 3 and 4 were evaluated numerically using $r = (l+1/2)/k$.[33]

In GLMT, the scattering amplitudes S_1 and S_2 can be written as[11,14]

$$S_1(\theta,\phi) = \sum_{l=1}^{\infty}\sum_{m=-l}^{l}\frac{2l+1}{l(l+1)}[(g_l^m)_{\mathrm{TM}}a_l m\pi_l^{|m|}(\theta) + i(g_l^m)_{\mathrm{TE}}b_l\tau_l^{|m|}(\theta)]e^{im\phi}, \tag{5}$$

$$S_2(\theta,\phi) = \sum_{l=1}^{\infty}\sum_{m=-l}^{l}\frac{2l+1}{l(l+1)}[i(g_l^m)_{\mathrm{TE}}b_l m\pi_l^{|m|}(\theta) + (g_l^m)_{\mathrm{TM}}a_l\tau_l^{|m|}(\theta)]e^{im\phi}, \tag{6}$$

where a_l and b_l are the Mie scattering coefficients (Ref. 9, p. 101)

$$a_l = \frac{n\psi_l(n\alpha)\psi_l'(\alpha) - \psi_l(\alpha)\psi_l'(n\alpha)}{n\psi_l(n\alpha)\xi_l'(\alpha) - \xi_l(\alpha)\psi_l'(n\alpha)}, \tag{7}$$

$$b_l = \frac{\psi_l(n\alpha)\psi_l'(\alpha) - n\psi_l(\alpha)\psi_l'(n\alpha)}{\psi_l(n\alpha)\xi_l'(\alpha) - n\xi_l(\alpha)\psi_l'(n\alpha)}, \tag{8}$$

and $\pi_l^{|m|}$ and $\tau_l^{|m|}$ are the angular functions[14]

$$\pi_l^{|m|}(\theta) = \frac{P_l^{|m|}(\cos\theta)}{\sin\theta}, \tag{9}$$

$$\tau_l^{|m|}(\theta) = \frac{\mathrm{d}}{\mathrm{d}\theta}P_l^{|m|}(\cos\theta). \tag{10}$$

In Eqs. 7 and 8, the relative refractive index is $n = n_s/n_0$ where n_s is the, in general, complex refractive index of the sphere and n_0 is the refractive index of the medium, the size parameter is $\alpha = ka$ where a is the radius of the sphere, and the functions $\xi_l = \psi_l - i\chi_l$, ψ_l, and χ_l are Ricatti-Bessel functions. The infinite series in Eqs. 5 and 6 were truncated at the integer closest to $\alpha + 4\alpha^{1/3} + 2$ during all calculations (Ref. 9, p. 477).

Following Bohren and Huffman (Ref. 9, p. 113), parallel ($i_\parallel$) and perpendicular ($i_\perp$) functions of the scattered irradiance per unit incidence irradiance (a dimensionless quantity) are defined using the scattering amplitudes (Eqs. 5 and 6) and a consideration of the polarization of the incident Bessel beam (Eqs. 1 and 2)

$$i_\parallel(\theta) = |S_2(\theta,\phi = 0^\circ)|^2, \tag{11}$$

$$i_{\perp}(\theta) = |S_1(\theta, \phi = 90^{\circ})|^2. \tag{12}$$

In these equations the angle ϕ has been chosen so that the Bessel beam described by Eqs. 1 and 2 will be polarized either parallel (Eq. 11) or perpendicular (Eq. 12) to the scattering plane. The scattering planes associated with $i_{\parallel}$ and $i_{\perp}$ are shown in Fig. 2a and b, respectively.

3 Results and Discussion

3.1 General features of Bessel beam scattering

Fig. 3 shows the angular scattered irradiance, the parallel and perpendicular scattering components, for a sphere with $\alpha = 30$ and $n = 1.33$ in a Bessel beam. The scattering is plotted as a function of both θ and θ_0. In all cases here, spheres were centred on the propagation axis of a Bessel beam. The justification for this choice is that this is where the potential energy of the sphere in a zeroth-order Bessel beam will be at its global minimum[19,22,26,40] and it should therefore be the most relevant position for practical applications.

The most distinctive feature of both the parallel and perpendicular polarization plots is the intense ridge of scattering that begins at $\theta = \theta_0 = 0°$, cuts across the plots in a nearly straight line, and ends at $\theta = \theta_0 = 90°$. To explore these ridges further, vertical slices of Fig. 3a and b were taken at a constant θ_0, generating multiple plots that were only a function of θ. Examining the angles of maxima in these slices, a peak always occurred at $\theta \approx \theta_0$ except for small θ_0. This peak is always one of the most intense maxima in a vertical slice and is often a global maximum at large θ_0. In the classical LMT, one would not expect a peak other than at $\theta = 0°$, the forward scattering direction, to be the strongest in an angular scattering plot. This is because the scattering of a plane wave by a sphere will be by far the most intense in the forward direction, particularly for large size parameters (see Ref. 9, p. 115). While we are not dealing with plane wave illumination here, this result from LMT can provide an intuitive basis for understanding the Bessel beam scattering. A common description of a Bessel beam is that of a superposition of plane waves propagating on a cone with a semi-apex angle θ_0 (Fig. 1).[41] Thus, the forward direction for such plane waves is not $\theta = 0°$ but rather $\theta = \theta_0$. With this

description and a consideration of scattering results from LMT, it therefore seems reasonable to expect that the scattering of a sphere by a Bessel beam would be very intense at $\theta \approx \theta_0$.

The above results are not consistent with results recently presented by Li *et al.*[34] There, a similar trend was observed, but only for calculations where $\theta_0 < 42°$. At higher angles, the ridge was no longer located at $\theta \approx \theta_0$ and instead was found at $\theta < \theta_0$. The origin of the discrepancy between our results and those of Li *et al.* is the manner in which the calculations were performed. Li *et al.* derived an analytical formula for the beam-shape coefficients by solving Eqs. 3 and 4 with the fields in Eqs. 1 and 2 using the integral localized approximation. Here, such an approximation was not used and Eqs. 3 and 4 were instead integrated numerically. During testing we found that the beam-shape coefficients of Li *et al.* did not agree with the beam-shape coefficients found through numerical integration for cases outside of the paraxial limit. Therefore, there is most likely a problem with the beam-shape coefficients presented in Ref. 34 and we recommend that their use be avoided.

A second feature of Fig. 3 is the undulation in scattered irradiance that occurs throughout both plots. For instance, these intensity variations lead to a checkerboard type pattern in the rectangular region of $\theta_0 = 25$ to $50°$ and $\theta = 130$ to $155°$ in Fig. 3a. Intensity undulations with similar periodicities are seen at all angles in both plots although they do not always form such visually distinct patterns. A vertical slice at any θ_0 always generates a scattering plot in θ that contains maxima and minima. Therefore, regardless of θ_0, it should always be possible to determine the size of a particle using angular scattering. It is also interesting to note that taking a horizontal slice at a fixed θ and generating a scattering plot as a function of θ_0 would contain intensity undulations with similar periodicities to those of the vertical slices. As a result, it should also be possible to determine particle size by measuring the scattering at a fixed θ while

θ_0 is varied. Such a measurement would be impractical with current instrumentation and it is much easier to take measurements over a wide range of θ at a fixed θ_0. These measurements as a function of θ_0 will not be discussed any further here.

3.2 Comparison between plane wave and Bessel beam scattering

Angular scattering plots are shown in Fig. 4 for spheres with $n = 1.33$ and at several different size parameters α in Bessel beams with various θ_0. These calculations were performed for polarizations both parallel and perpendicular to the scattering plane. Of the five different θ_0 chosen in Fig. 4, one gives results that are identical to plane wave scattering ($\theta_0 = 0°$) while the others cover the range typically used in aerosol optical Bessel traps (except $\theta_0 = 30°$, which is considerably larger than the maximum θ_0 that has been used).[23–29]

Our analysis will focus on the conditions under which the scattering in a Bessel beam deviates significantly from that of a plane wave. For small θ_0, the first intensity minimum of the non-paraxial zeroth-order Bessel beam will occur approximately at the dimensionless parameter

$$r_0 = \frac{2.40483}{\sin\theta_0}, \tag{13}$$

which corresponds to the first root of the zeroth-order Bessel function. The parameter $r_0 = k\rho_0$ where ρ_0 is the radial distance between the centre of the beam and the first intensity minimum, which is commonly referred to as the central core size of a zeroth-order Bessel beam.[19,42] The parameter r_0 is used here to define a scaled size $\gamma = \alpha/r_0$. As γ increases from zero to one, the size parameter of the sphere approaches the first intensity minimum of the Bessel beam and it is expected that the associated angular scattering will deviate significantly from that of a plane wave.

Pearson's correlation coefficients c were calculated between the angular scattering of a plane wave ($\theta_0 = 0°$) and the angular scattering of Bessel beams with various θ_0. For a data set containing N pairs (x_i, y_i) the correlation coefficient is

$$c = \frac{N\sum x_i y_i - \sum x_i \sum y_i}{\sqrt{N\sum x_i^2 - (\sum x_i)^2}\sqrt{N\sum y_i^2 - (\sum y_i)^2}}. \tag{14}$$

In the analysis here, each (x_i, y_i) consists of the scattered intensity of the plane wave and the Bessel beam at the same angle. The set $(x_1, y_1), (x_2, y_2), \ldots, (x_N, y_N)$ spans the angular range of interest.

Table 1 lists the correlations for all of the $\theta_0 \neq 0°$ plots shown in Fig. 4 with their corresponding $\theta_0 = 0°$ (plane wave) plot. In the following discussion, a value of $c = 0.99900$ is chosen to be the lower limit at which angular scattering for the Bessel system is no longer well described by plane wave scattering. In Fig. 4, pairs of curves whose c is below this limit have shapes that are easy to distinguish visually from that of a plane wave as they contain shifts in extrema that are greater than 1°. Notably, the parallel scattering component from a particle of $\alpha = 1$ that is illuminated by a Bessel beam with $\theta_0 = 30°$ has a value of $c = 0.99899$, just below this threshold. The location of the intensity minimum in that plot is shifted by about 1.5° from the $\alpha = 1$ plane wave curve for the same polarization. In comparison, the perpendicular scattering component from a particle of $\alpha = 1$ that is illuminated by a Bessel beam with $\theta_0 = 30°$ has a value of $c = 0.99987$, above the chosen threshold value of c. The reason for this is that, unlike other curves in Fig. 4 that fall below the threshold value of c, there are no shifts in extrema for this curve. These two examples serve to qualitatively illustrate the level of divergence or agreement between plane wave and Bessel beam illumination expected for the chosen threshold value of c.

For $\theta_0 < 10°$, it was found through additional calculations that c typically falls below 0.999 once γ increases to within the range of 0.4 to 0.6. Indeed, the intensity profile across a sphere is far from uniform when γ is between 0.4 and 0.6. As an example of this non-uniformity, we compare the intensity of the Bessel beam at $\rho = a$ (the surface of the sphere) when $z = 0$ to the intensity of the Bessel beam at $\rho = 0$ (the center of the sphere). The relative intensities are ~ 0.61 when $\gamma = 0.4$ and ~ 0.30 when $\gamma = 0.6$. Therefore, it is somewhat surprising that the scattering from systems with large values of γ can still correlate strongly with illumination by a plane wave. Regardless, this result is fortuitous for certain practical applications. Specifically, the assumption of plane wave scattering can be used for particles whose size is less than (and even approaches) the core size when attempting to determine the size and refractive index of a spherical particle in a Bessel beam by fitting the angular scattered light intensity. This will greatly reduce the computational time as beam-shape coefficients do not need to be solved numerically in such cases.

3.3 Fitting angular scattering using plane waves

The correlation between plane wave and Bessel beam scattering was investigated further by preparing a series of simulated angular scattering plots for a homogeneous sphere in a Bessel beam. Several sets of data were generated at $\theta_0 = 5$ and $10°$ for three different angular scattering ranges. Fig. 5 shows the relationship between the actual value of γ for the sphere in the Bessel beam versus the fitted value of γ found. The fitted value of γ was found by first maximizing c between the Bessel beam and plane wave scattering by varying a in the plane wave scattering calculation (n was fixed at 1.33), then dividing this value of a by the core size of the Bessel beam, ρ_0 (so technically a is fitted and γ is calculated from that result). For the angular range

of $\theta = 0$ and 180° it can be seen that the fitting using plane wave scattering will be satisfactory up to $\gamma \simeq 0.4$ (for both values of θ_0 and either polarization). Beyond that point, though, the calculated values of γ begin to deviate from a straight line with a slope of one (the grey curves in Fig. 5). Thus, at least in these two examples, fitting the angular scattering from a particle in a Bessel beam with $\lambda = 532$ nm using plane wave scattering would be satisfactory if a was known to be less than ~ 935 nm if $\theta_0 = 5°$ ($\rho_0 = 2336$ nm) or less than ~ 469 nm if $\theta_0 = 10°$ ($\rho_0 = 1173$ nm). It can also be seen in Fig. 5 for the angular range of $\theta = 0$ and 180° that for γ up to ~ 0.75, estimating the droplet size through a comparison of the simulated data to angular scattering calculations using a plane wave can provide a rough estimate of size. Again, with $\lambda = 532$ nm this value of γ corresponds to an upper limit on a of ~ 1752 nm if $\theta_0 = 5°$ or ~ 879 nm if $\theta_0 = 10°$. For $\gamma > 0.75$, fitting angular scattering with a plane wave should be avoided. The fitting process described here was also repeated for $n = 1.4$, 1.5, and 1.6 (not shown here). For these systems, plane wave fitting was also found to be satisfactory for γ up to ~ 0.4 when $\theta = 0$ to 180°.

In practice, it is not possible to measure light scattering over the full range of $\theta = 0$ to 180°. To investigate the effect of limiting the angular range, two additional cases are considered in Fig. 5: $\theta = 70$ to 110° and $\theta = 80$ to 100°. The angular range of $\theta = 70$ to 110° is a fair representation of what is typically possible to measure in current Bessel beam experiments.[23–28] Surprisingly, for $\theta_0 = 5°$, the fits for $\theta = 70$ to 110° are overall more accurate than their counterparts found using $\theta = 0$ to 180° when $\gamma < 0.75$. However, the same statement is not true for $\theta_0 = 10°$, as the parallel polarization in the $\theta = 70$ to 110° case contains several regions where the best-fit is significantly worse than the fit obtained using $\theta = 0$ and 180°. The other angular range considered in Fig. 5 is $\theta = 80$ to 100°. The fitting results are similar to those in the $\theta = 70$

to 110° plots, however they do contain more scatter. Overall, if n is known and the angular scattering is measured over a range that is typically used in Bessel beam trapping (e.g. $\theta = 70$ to 110°), plane wave fitting can be used even for fairly high values of γ provided that θ_0 is not too large (e.g. $\theta_0 = 5°$ is satisfactory but $\theta_0 = 10°$ is not).

3.4 The mean correlation method for fitting radius and refractive index from angular scattering

The analysis performed in Fig. 5 was limited to cases where n is known during the fitting. In many experimental situations, this information is not known and it will be desirable to simultaneously characterize both a and n using light scattering. The effect of θ_0 on such a fitting process is shown in Fig. 6 (for $\theta = 70$ to 110°). Here, γ and n were found by maximizing c between the Bessel beam and plane wave scattering by simultaneously varying both a and n. This was accomplished by constructing a c hypersurface as a function of a and n across the parameter ranges of a from 1 to 3000 nm and n from 1.25 to 1.40. For each angular scattering plot, the values of a and n that maximized c could then be found by searching this surface. The outcome of the fitting process for γ is similar to what was seen in the $\theta = 70$ to 110° results in Fig. 5. While there is more scatter in Fig. 6 for both $\theta_0 = 5$ and 10°, the fitting procedure is still able to provide a rough assessment of γ. However, this is not the case for the fitted values of n. The accuracy of the n fits is very poor across the entire range of γ used here. In fact, the accuracy would actually be worse if the search space for n had not been restricted from 1.25 to 1.40. It is also problematic that many of the best-fits that contain inaccurate values n also have c that are very close to one, so there is no simple way to disregard these values. Note that this result is not unique to the situation studied here (i.e. fitting Bessel beam scattering using plane

wave scattering) and similar difficulties are often encountered in a variety of situations when trying to characterize particles using angular light scattering. Consider an example where the incident beam is well-described as being a plane wave and the sphere has values of α and n that are similar to those studied here. If the scattering is fitted using LMT, under ideal conditions it is expected that there should be no difficulty in determining n. However, if the angular range used in the fitting contains a small systematic error (e.g. scattering is collected over $\theta = 69$ to 109° but is fitted using $\theta = 70$ to 110°), then best-fits similar to those seen in Fig. 6 may be obtained. Therefore, even when fitting plane wave scattering using plane waves, it may not be possible to accurately determine n if there is a small error in parameters used to describe the system.

Here, we propose a different method to more accurately determine a and n. In a typical single particle experiment, multiple angular scattering plots (henceforth referred to as 'frames') will be collected over time as the particle size and composition evolves. We define $c_i(a_i, n)$ to be the maximized correlation between the observed and calculated angular scattering for frame i. The radius a_i is the value of a that maximizes the correlation for frame i at a fixed n. When the same n is used across all N frames, the set of maximized correlations will be $c_1(a_1, n), c_2(a_2, n), \ldots, c_N(a_N, n)$. The mean of this set of maximized correlations is then

$$\bar{c}(n) = \frac{1}{N} \sum_{i=1}^{N} c_i(a_i, n). \tag{15}$$

The refractive index of best-fit can then be found by maximizing $\bar{c}(n)$ with respect to n. Note that for each value of n, an entirely new set of $c_1(a_1, n), c_2(a_2, n), \ldots, c_N(a_N, n)$ must be calculated.

To investigate the accuracy of Eq. 15, angular scattering by a sphere in a Bessel beam was

simulated for systems where $n = 1.33$ and $\lambda = 532$ nm. Four sets of frames were generated at $\theta_0 = 5$ and 10° across an angular range of $\theta = 70$ to 110° for both parallel and perpendicular polarizations. For the two sets of frames where $\theta_0 = 5^\circ$, the range of a was 500 to 1500 nm and, for the two sets of frames where $\theta_0 = 10^\circ$, the range of a was 250 to 750 nm. In all sets, frames were generated across their respective ranges of a in steps of 1 nm. Fig. 7 shows $\bar{c}(n)$ for these simulated sets of frames when they are fitted using plane wave scattering. For $\theta_0 = 5^\circ$, the values of n that maximize $\bar{c}(n)$ are 1.3308 and 1.3408 for the parallel and perpendicular polarizations, respectively, and, for $\theta_0 = 10^\circ$, 1.3486 and 1.3206 for the parallel and perpendicular polarizations, respectively.

In contrast to the method of maximizing $\bar{c}(n)$, the fitting method in Section 3.3 determines the a and n of best-fit in each frame independently of the other frames. As was shown in Fig. 6, this leads to significant scatter in the best-fits for n. However, it may be possible that if averaging is then performed across all frames results similar to maximizing Eq. 15 will be obtained. To investigate this, the same sets of frames were fitted using the method described in Section 3.3. When the n of best-fit from each frame are averaged, the following results are obtained: for $\theta_0 = 5^\circ$, the average n of best-fit is 1.3290 for the parallel polarization and 1.3454 for the perpendicular polarizations and, for $\theta_0 = 10^\circ$, the average n of best-fit is 1.4573 for the parallel polarization and 1.3590 for the perpendicular polarization. Therefore, when determining the n of best-fit from multiple angular scattering plots, maximizing Eq. 15 does offer improvements to accuracy over the method described in Section 3.3.

Thus far we have restricted our discussion to spheres where n is independent of volume. For many systems this will not be true (e.g. a hygroscopic droplet that varies in a and n as the relative humidity changes). To treat such cases, it necessary to first express n as a function of

a,

$$n(a) = n_0 + \frac{n_1}{a^3} + \frac{n_2}{a^6} + \cdots + \frac{n_j}{a^{3j}}. \tag{16}$$

Then, the maximized mean correlation will be a function of the parameters $n_0, n_1, n_2, \ldots, n_j$:

$$\bar{c}(n_0, n_1, n_2, \ldots, n_j) = \frac{1}{N} \sum_{i=1}^{N} c_i(a_i, n_0, n_1, n_2, \ldots, n_j). \tag{17}$$

In order to maximize $\bar{c}(n_0, n_1, n_2, \ldots, n_j)$ a j-dimensional search must be performed. We are currently implementing such fitting methods for studies involving the hygroscopic behaviour of inorganic aerosols.

4 Conclusion

Elastic light scattering for a homogeneous sphere in an optical Bessel beam was investigated using GLMT. It was found that angular scattering was always very intense at $\theta \approx \theta_0$. Undulations in scattered intensity occurred as both a function of θ and θ_0. Correlation coefficients between the angular scattering of a Bessel beam and a plane wave were also calculated for several systems. A key conclusion is that when the ratio of the sphere size to the core size of the Bessel beam is less than ~ 0.75, the angular scattering of the Bessel beam correlated strongly to that of a plane wave provided that (i) θ_0 is not too large, (ii) light is collected over an angular range found in typical experiments, and (iii) the relative refractive index of the particle is known. Finally, the characterization of spherical particles (determination of both radius and relative refractive index) using angular light scattering was discussed and a mean correlation method was proposed. This fitting method was shown to provide increased accuracy in the determination of the relative refractive index over a simpler method where angular scattering plots in a set of collected data are analyzed independently of each other.

Acknowledgements

JPR acknowledges financial support from the Engineering and Physical Sciences Research Council (EPSRC) through the support of a Leadership Fellowship (EP/G007713/1).

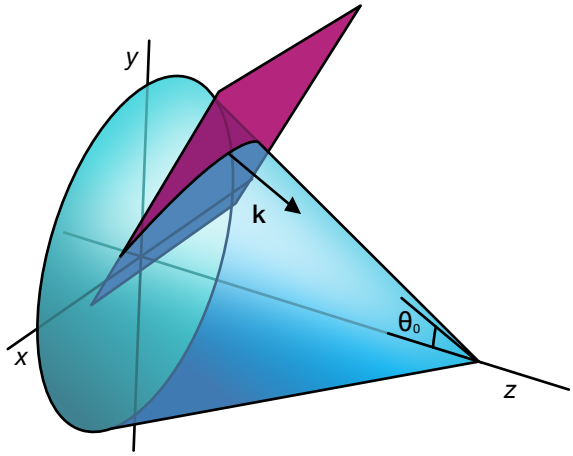

Figure 1: Illustration of a plane wave with a wavevector $\mathbf{k}$ propagating on the surface of a cone with a semi-apex angle θ_0. When such plane waves are evenly distributed over the surface of the cone (across all azimuthal angles), their superposition forms a Bessel beam. The relationship between $\mathbf{k}$ and the wavenumbers used in Section 2 is $|\mathbf{k}|^2 = k^2 = k_z^2 + k_\perp^2$.

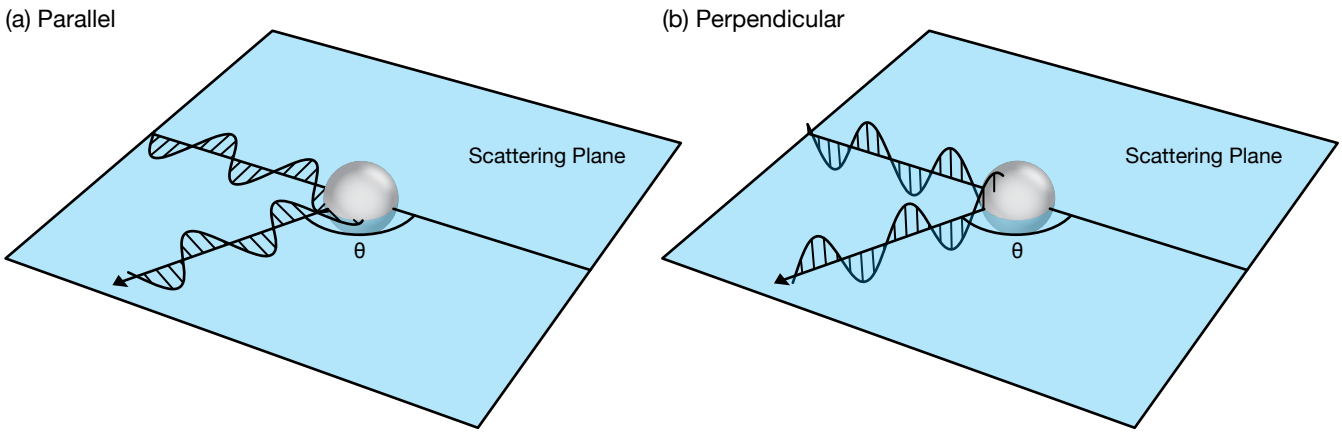

Figure 2: Illustration of light polarized (a) parallel and (b) perpendicular to the scattering plane and the definition of the scattering angle θ relative to the incident and scattered light. The dimensionless quantities $i_{\parallel}$ and $i_{\perp}$ correspond to light in (a) and (b), respectively.

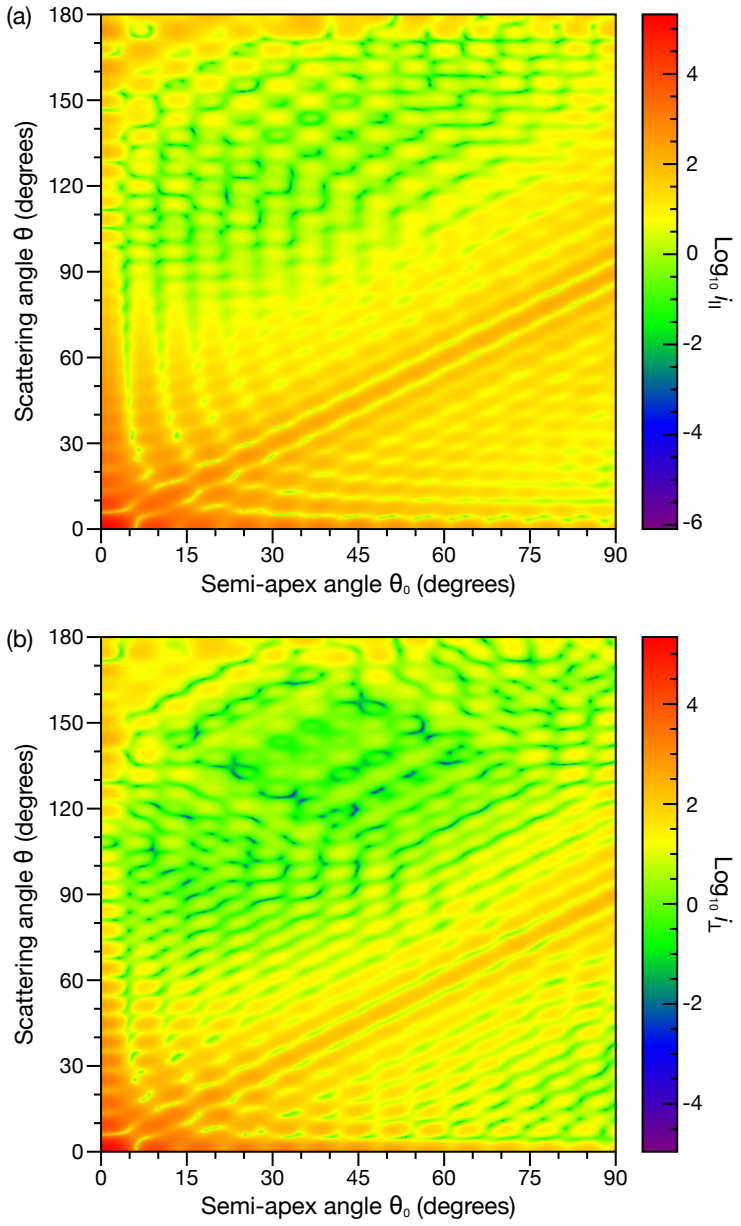

Figure 3: Scattered intensity as a function of both the semi-apex angle θ_0 and the scattering angle θ for incident light polarized (a) parallel and (b) perpendicular to the scattering plane. In both calculations, $\alpha = 30$ and $n = 1.33$.

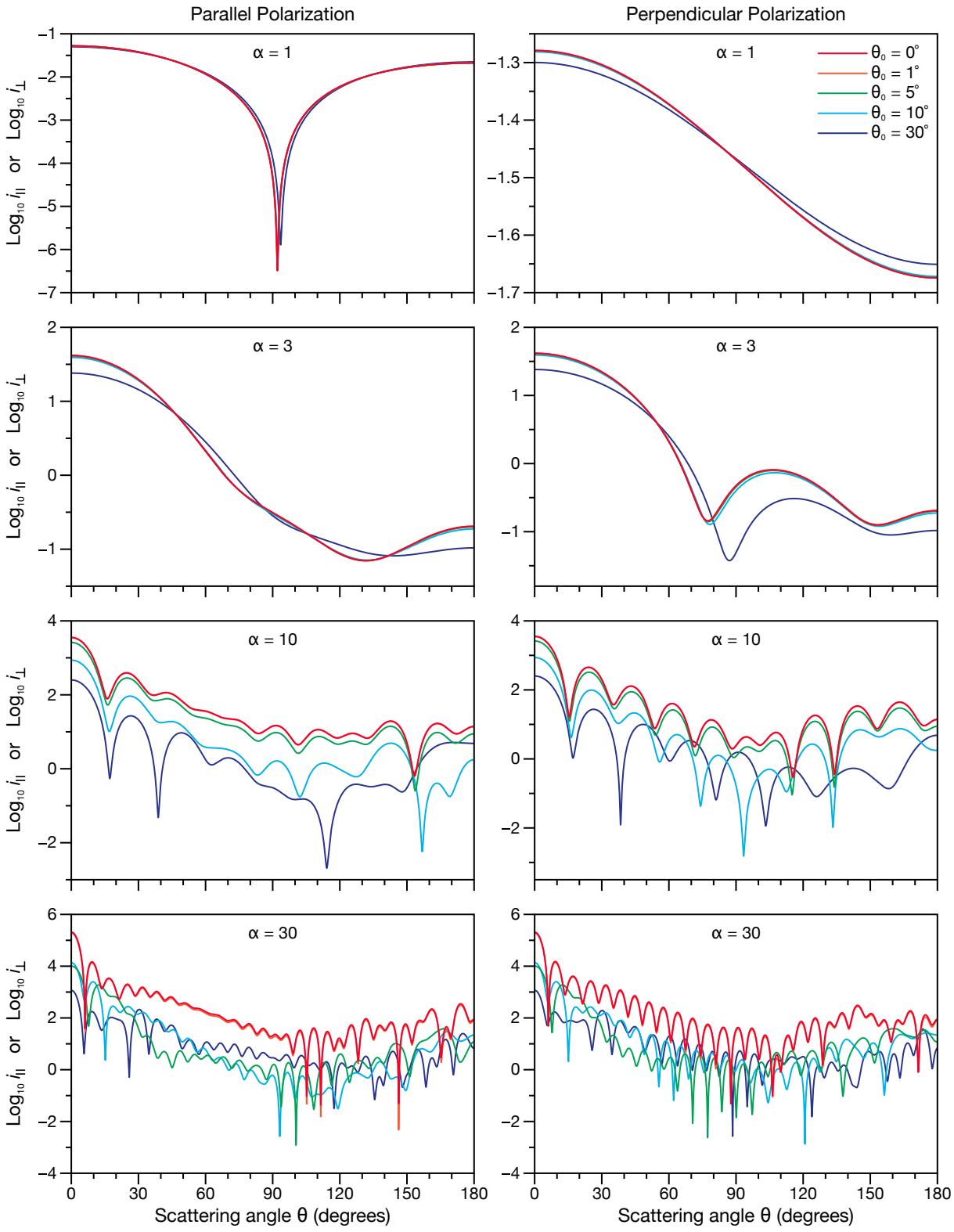

Figure 4: Scattered intensity as a function of θ for several different α and θ_0. In all cases, $n = 1.33$. For plots in the left column, incident light is polarized parallel to the scattering plane. For plots in the right column, incident light is polarized perpendicular to the scattering plane.

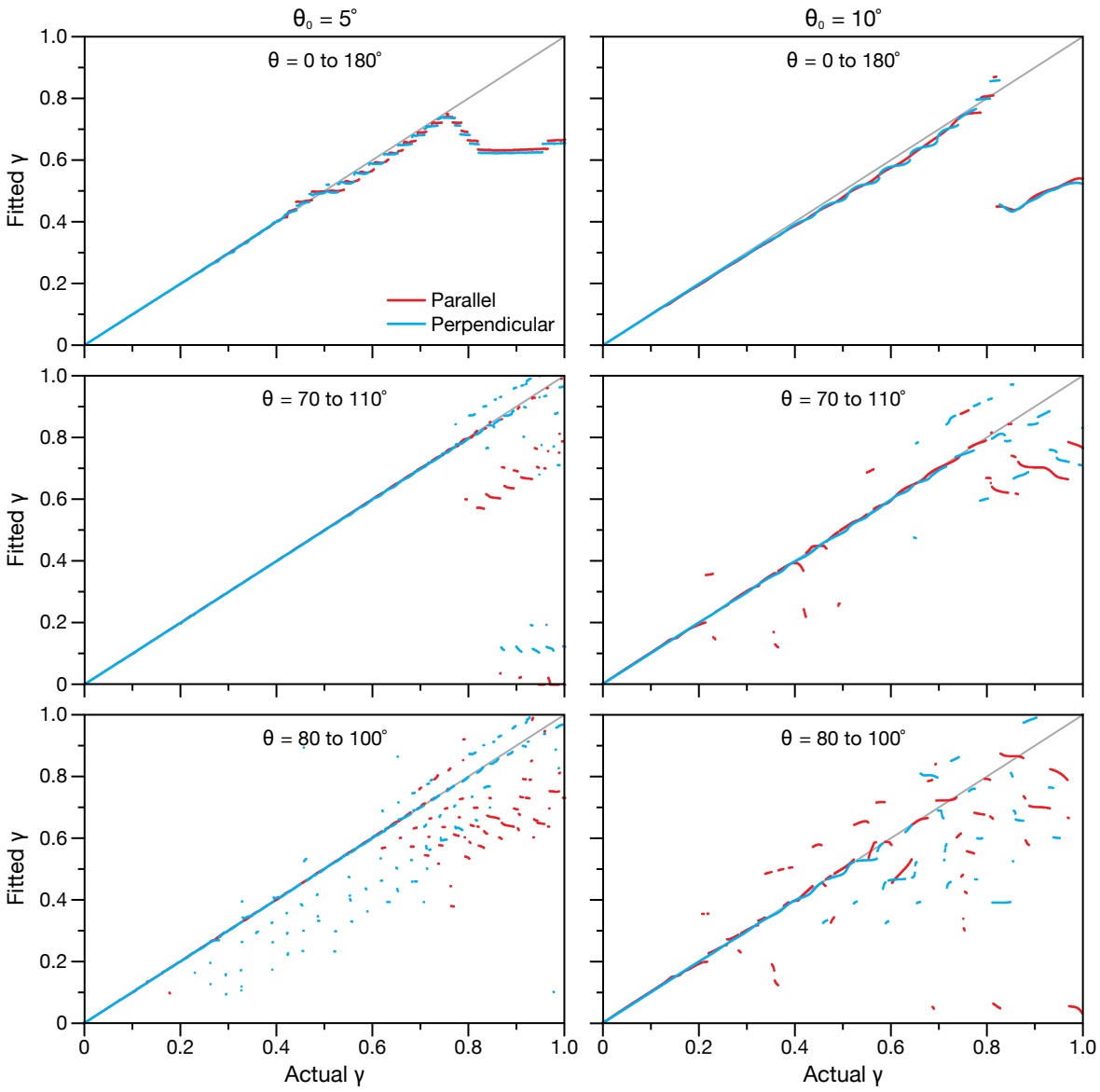

Figure 5: Best fits for angular scattering from a sphere in a Bessel beam with $\theta_0 = 5°$ and $\theta_0 = 10°$ using plane wave scattering. The range of θ used during calculations was either 0 to 180°, 70 to 110°, or 80 to 100°. In all cases, n was 1.33. In order to generate and fit the angular scattering plots, the wavelength of the incident beam was fixed at $\lambda = 532$ nm. Then, angular scattering from the sphere in a Bessel beam was calculated across the range of θ for a from either 1 to 2336 nm in 1 nm steps for $\theta_0 = 5°$ or from 1 to 1173 nm in 1 nm steps for $\theta_0 = 10°$. Best-fits were then found using plane wave scattering and by varying a until c was maximized. For presentation here, all a are converted to γ. Fittings were performed for both parallel and perpendicular polarization. Grey lines are drawn to guide the eye to where the points should fall if the fitted γ matches the actual γ.

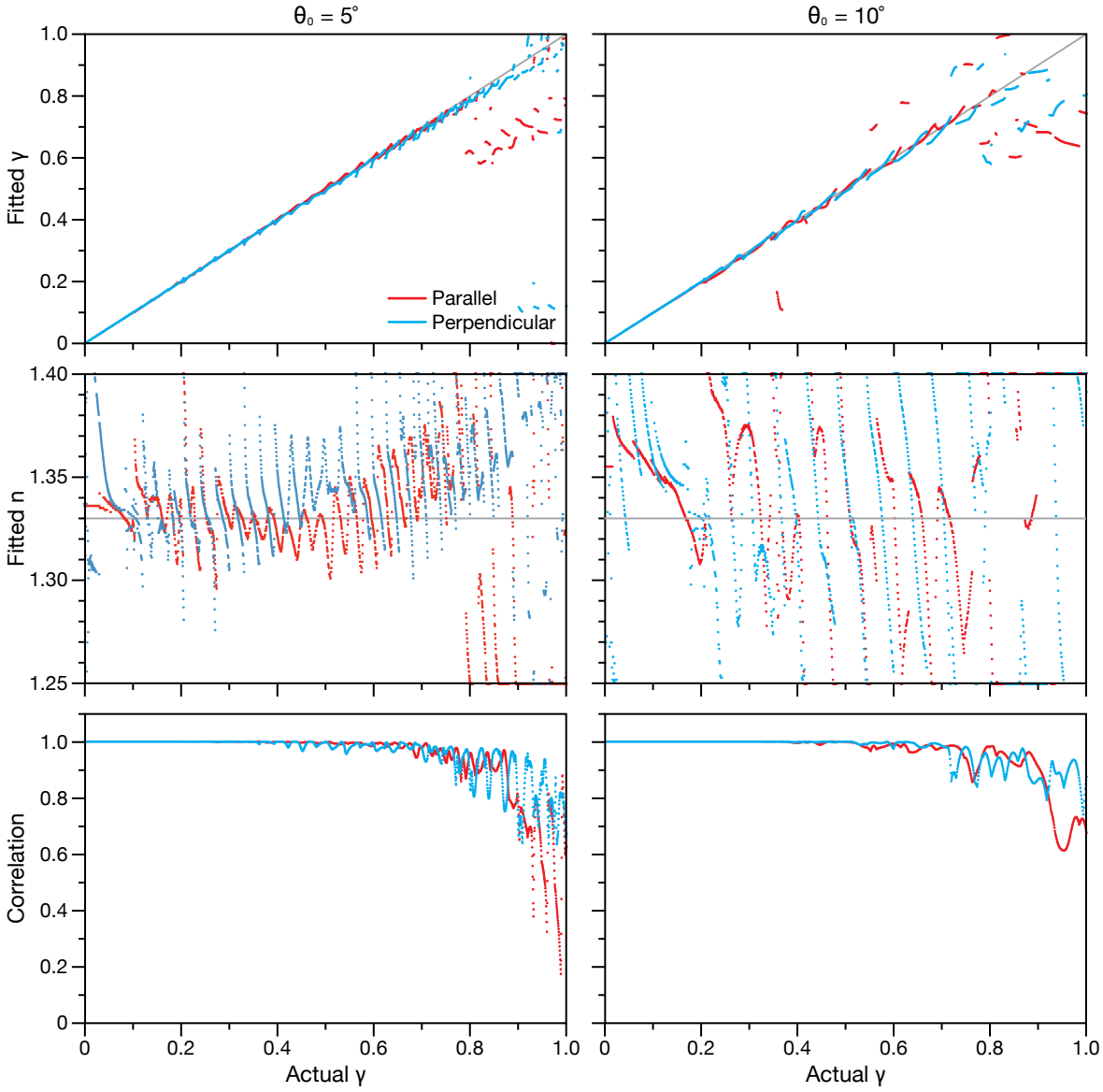

Figure 6: Best fits for angular scattering from a sphere in a Bessel beam with $\theta_0 = 5°$ and $\theta_0 = 10°$ using plane wave scattering. The range of θ used during calculations was 70 to 110°. The method for generating angular scattering plots is identical to that which is described in the caption of Fig. 5. Best-fits were found using plane wave scattering and by varying a and n until c was maximized. For presentation here, all a are converted to γ. Fittings were performed for both parallel and perpendicular polarization. The search space for n was restricted between 1.25 and 1.40. Grey lines are drawn to guide the eye to where the points should fall if the fitted values match the actual values.

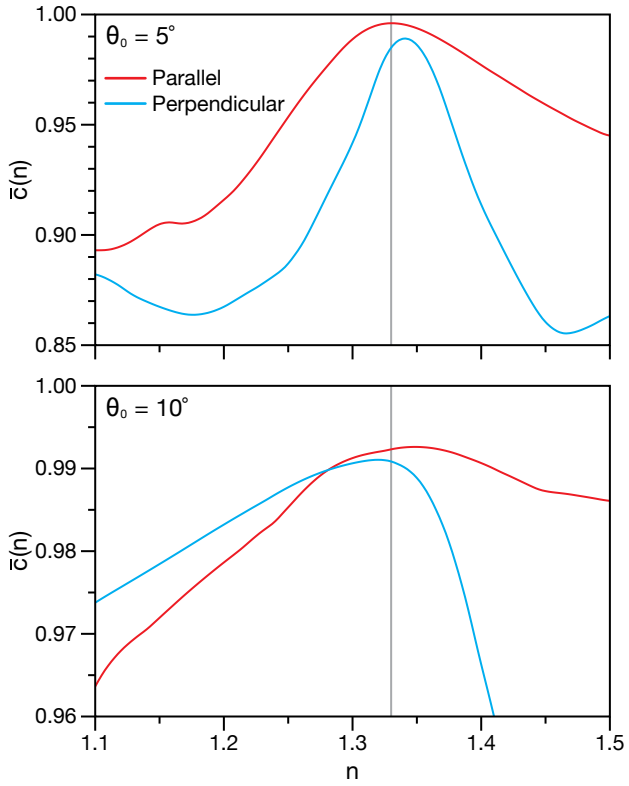

Figure 7: Mean maximized correlation $\bar{c}(n)$ between Bessel beam scattering ($\theta_0 = 5°$ and $\theta_0 = 10°$) and plane wave scattering. The range of θ used during calculations was 70 to 110°. The Bessel beam angular scattering plots were generated using $\lambda = 532$ nm and $n = 1.33$ over a range of $a = 500$ to 1500 nm for $\theta_0 = 5°$ and $a = 250$ to 750 nm for $\theta_0 = 10°$ (in both cases using a step size of 1 nm). Calculations were performed for both parallel and perpendicular polarization. Grey lines are added to both plots to indicate the location of the actual n.

Table 1: Correlation coefficients c between the angular scattering of a plane wave ($\theta_0 = 0°$) and the corresponding angular scattering in a Bessel beam ($\theta_0 \neq 0°$) for the plots in Fig. 4.

	$i_{\parallel}$				$i_{\perp}$			
α	$\theta_0 = 1°$	$5°$	$10°$	$30°$	$1°$	$5°$	$10°$	$30°$
1	1.00000	1.00000	0.99999	0.99899	1.00000	1.00000	1.00000	0.99987
3	1.00000	1.00000	0.99992	0.99108	1.00000	1.00000	0.99996	0.99535
10	1.00000	0.99996	0.99881	0.99712	1.00000	0.99994	0.99824	0.99389
30	0.99999	0.95448	0.98849	0.96246	0.99999	0.95425	0.98869	0.96907

References

1. L. Lorenz, *Oeuvres Scientifiques de L. Lorenz, Revues et Annotées par H. Valentiner* (Librairie Lehmann & Stage, 1898), p. 405.

2. G. Mie, "Beiträge zur optik trüber medien, speziell kolloidaler metallösungen," Ann. Phys. **330**, 377-445 (1908).

3. R. Fuchs and K. L. Kliewer, "Optical modes of vibration in an ionic crystal sphere," J. Opt. Soc. Am. **58**, 319-330 (1968).

4. A. Ashkin and J. M. Dziedzic, "Observation of resonances in the radiation pressure on dielectric spheres," Phys. Rev. Lett. **38**, 1351-1354 (1977).

5. S. Underwood and P. Mulvaney, "Effect of the solution refractive index on the color of gold colloids," Langmuir **10**, 3427-3430 (1994).

6. T. Klar, M. Perner, S. Grosse, G. von Plessen, W. Spirkl, and J. Feldmann, "Surface-plasmon resonances in single metallic nanoparticles," Phys. Rev. Lett. **80**, 4249-4252 (1998).

7. M. S. Wheeler, J. S. Aitchison, and M. Mojahedi, "Three-dimensional array of dielectric spheres with an isotropic negative permeability at infrared frequencies," Phys. Rev. B **72**, 193103 (2005).

8. H. C. van de Hulst, *Light Scattering by Small Particles* (Wiley, 1957).

9. C. F. Bohren and D. R. Huffman, *Absorption and Scattering of Light by Small Particles* (John Wiley and Sons, 1983).

10. J. P. Barton, D. R. Alexander, and S. A. Schaub, "Internal and near-surface electromagnetic fields for a spherical particle irradiated by a focused laser beam," J. Appl. Phys. **64**, 1632-1639 (1988).

11. G. Gouesbet, B. Maheu, and G. Gréhan, "Light scattering from a sphere arbitrarily located in a Gaussian beam, using a Bromwich formulation," J. Opt. Soc. Am. A **5**, 1427-1443 (1988).

12. J. P. Barton, D. R. Alexander, and S. A. Schaub, "Internal fields of a spherical particle illuminated by a tightly focused laser beam: focal point positioning effects at resonance," J. Appl. Phys. **65**, 2900-2906 (1989).

13. J. P. Barton, D. R. Alexander, and S. A. Schaub, "Theoretical determination of net radiation force and torque for a spherical particle illuminated by a focused laser beam," J. Appl. Phys. **66**, 4594-4602 (1989).

14. J. A. Lock and G. Gouesbet, "Rigorous justification of the localized approximation to the beam-shape coefficients in generalized Lorenz-Mie theory. I. On-axis beams," J. Opt. Soc. Am. A **11**, 2503-2515 (1994).

15. G. Gouesbet and J. A. Lock, "Rigorous justification of the localized approximation to the beam-shape coefficients in generalized Lorenz-Mie theory. II. Off-axis beams," J. Opt. Soc. Am. A **11**, 2516-2525 (1994).

16. J. A. Lock and G. Gouesbet, "Generalized Lorenz-Mie theory and applications," J. Quant. Spectrosc. Radiat. Transfer **110**, 800-807 (2009).

17. G. Gouesbet, J. A. Lock, and G. Gréhan, "Generalized Lorenz-Mie theories and description of electromagnetic arbitrary shaped beams: Localized approximations and localized beam models, a review," J. Quant. Spectrosc. Radiat. Transfer **112**, 1-27 (2011).

18. J. Durnin, J. J. Miceli, and J. H. Eberly, "Diffraction-free beams," Phys. Rev. Lett. **58**, 1499-1501 (1987).

19. D. Mcgloin and K. Dholakia, "Bessel beams: Diffraction in a new light," Contemp. Phys. **46**, 15-28 (2005).

20. T. Čižmár, V. Kollárová, Z. Bouchal, and P. Zemánek, "Sub-micron particle organization by self-imaging of non-diffracting beams," New J. Phys. **8**, 43 (2006).

21. T. Čižmár, M. Šiler, and P. Zemánek, "An optical nanotrap array movable over a milimetre range," Appl. Phys. B **84**, 197-203 (2006).

22. G. Milne, K. Dholakia, D. McGloin, K. Volke-Sepulveda, and P. Zemánek, "Transverse particle dynamics in a Bessel beam," Opt. Express **15**, 13972-13987 (2007).

23. H. Meresman, J. B. Wills, M. Summers, D. McGloin, and J. P. Reid, "Manipulation and characterisation of accumulation and coarse mode aerosol particles using a Bessel beam trap," Phys. Chem. Chem. Phys. **11**, 11333-11339 (2009).

24. A. E. Carruthers, J. P. Reid, and A. J. Orr-Ewing, "Longitudinal optical trapping and sizing of aerosol droplets," Opt. Express **18**, 14238-14244 (2010).

25. A. E. Carruthers, J. S. Walker, A. Casey, A. J. Orr-Ewing, and J. P. Reid, "Selection and characterization of aerosol particle size using a Bessel beam optical trap for single particle analysis," Phys. Chem. Chem. Phys. **14**, 6741-6748 (2012).

26. T. C. Preston, B. J. Mason, J. P. Reid, D. Luckhaus, and R. Signorell, "Size-dependent position of a single aerosol droplet in a Bessel beam trap," J. Opt. **16**, 025702 (2014).

27. M. I. Cotterell, B. J. Mason, A. E. Carruthers, J. S. Walker, A. J. Orr-Ewing, and J. P. Reid, "Measurements of the evaporation and hygroscopic response of single fine-mode aerosol particles using a Bessel beam optical trap," Phys. Chem. Chem. Phys. **16**, 2118-2128 (2014).

28. J. W. Lu, A. M. J. Rickards, J. S. Walker, K. J. Knox, R. E. H. Miles, J. P. Reid, and R. Signorell, "Timescales of water transport in viscous aerosol: measurements on sub-micron particles and dependence on conditioning history," Phys. Chem. Chem. Phys. **16**, 9819-9830 (2014).

29. B. J. Mason, J. S. Walker, J. P. Reid, and A. J. Orr-Ewing, "Deviations from plane-wave Mie scattering and precise retrieval of refractive index for a single spherical particle in an optical cavity," J. Phys. Chem. A **118**, 2083-2088 (2014).

30. J. D. Eversole, H. B. Lin, A. L. Huston, A. J. Campillo, P. T. Leung, S. Y. Liu, and K. Young, "High-precision identification of morphology-dependent resonances in optical processes in microdroplets," J. Opt. Soc. Am. B **10**, 1955-1968 (1993).

31. T. C. Preston and J. P. Reid, "Accurate and efficient determination of the radius, refractive index, and dispersion of weakly absorbing spherical particle using whispering gallery modes," J. Opt. Soc. Am. B, **30**, 2113-2122 (2013).

32. J. M. Taylor and G. D. Love, "Multipole expansion of Bessel and Gaussian beams for Mie scattering calculations," J. Opt. Soc. Am. A, **26**, 278-282 (2009).

33. L. A. Ambrosio and H. E. Hernández-Figueroa, "Integral localized approximation description of ordinary Bessel beams and application to optical trapping forces," Biomed. Opt. Express **2**, 1893-1906 (2011).

34. R. Li, L. Guo, C. Ding, and Z. Wu, "Scattering of an axicon-generated Bessel beam by a sphere," Opt. Commun. **307**, 25-31 (2013).

35. F. G. Mitri, "Arbitrary scattering of an electromagnetic zero-order Bessel beam by a dielectric sphere," Opt. Lett. **36**, 766-768 (2011).

36. F. G. Mitri, "Electromagnetic Wave Scattering of a High-Order Bessel Vortex Beam by a Dielectric Sphere," IEEE Trans. Antennas Propag. **59**, 4375-4379 (2011).

37. T. Qu, Z.-S. Wu, Q.-C. Shang, Z.-J. Li, and L. Bai, "Electromagnetic scattering by a uniaxial anisotropic sphere located in an off-axis Bessel beam," J. Opt. Soc. Am. A **30**, 1661-1669 (2013).

38. Z. Cui, Y. Han, Z. Chen, and L. Han, "Scattering of Bessel beam by arbitrarily shaped composite particles with core-shell structure," J. Quant. Spectrosc. Radiat. Transfer **144**, 108-116 (2014).

39. T. Čižmár,"Optical traps generated by non-traditional beams," Ph.D. thesis, Masaryk University in Brno (2006). URL http://www.isibrno.cz/omitec/download.php?Cizmar-PhD-thesis.pdf.

40. S. Tatarkova, W. Sibbett, and K. Dholakia, "Brownian particle in an optical potential of the washboard type," Phys. Rev. Lett. **91**, 038101 (2003).

41. J. Durnin, "Exact solutions for nondiffracting beams. I. The scalar theory," J. Opt. Soc. Am. A **4**, 651-654 (1987).

42. O. Brzobohatý, T. Čižmár, and P. Zemánek, "High quality quasi-Bessel beam generated by round-tip axicon," Opt. Express **16**, 12688-12700 (2008).